



A nonlinear triboelectric nanogenerator with a broadened bandwidth for effective harvesting of vibration energy

Guoqiang Xu¹, Jingjing Fu¹, Chuanyang Li¹, Juntong Xing¹, Chaojie Chen¹, Wei-Hsin Liao¹, Zhonglin Wang²  and Yunlong Zi^{1,2,3,4,5,6} 

ABSTRACT

A narrow resonance bandwidth of an energy harvesters limits its response to the wide frequency spectrum in ambient environments. This work proposes an addition of a nonlinear restoring force applied to a triboelectric nanogenerator (TENG) to tune and broaden the resonance bandwidth. This restoring force is applied by permanent magnets at both sides of the slider and two external magnets. The noncontact strategy is adopted between the slider and the grating electrodes to avoid the wear of electrodes and energy loss caused by friction. The results show that compared with the linear system, the nonlinear noncontact TENG (NN-TENG) can increase the peak current from 6.3 μA to 7.89 μA , with an increment of about 25%, increase the peak power from 650 μW to 977 μW , increasing by about 50%, and increase the bandwidth from 0.5 Hz to 7.75 Hz, increasing by about 1400%. This work may enable a new strategy to boost the bandwidth and output power of TENG through nonlinear oscillators.

KEYWORDS

Nonlinear oscillator, triboelectric nanogenerator, electromechanical coupling model, energy harvester, dynamic performance, mechanical vibration.

Over the past decades, harvesting ambient energy has attracted increasing interest for realizing self-powered systems to meet large-scale energy demands^[1–5]. Searching for clean and renewable energy with reduced carbon emissions is urgent for the sustainable development of modern society^[6–9]. Mechanical vibration, as compared with other types of energy (heat, light, acoustics), is an attractive source due to its high availability in environments^[10]. Based on various energy conversion mechanisms, including piezoelectric^[11–13], electromagnetic^[14–16], and triboelectric^[17–22], wasted mechanical energy from vibrations has been transformed into useful electrical power. Usually, triboelectric nanogenerator (TENG) has the advantage to collect low-frequency energies, such as human body motion^[23], airflows^[24], and ocean^[25], which are commonly existing in the environment^[14,26,27]. For the TENG applications, four basic modes of TENG have been developed, including vertical contact-separation (CS) mode, lateral sliding (LS) mode, single-electrode (SE) mode, and freestanding triboelectric-layer (FT) mode^[28,29]. Each mode has specific structure and material(s) as well as triggering mechanisms. Among them, the sliding FT (SFT) mode has the highest output energy density and is frequently used as the main structure for harvesting energy^[30]. However, the bandwidth of SFT mode TENG is usually narrow which greatly limits its application scope^[30,31].

To solve the issue of narrow response bandwidth, the nonlinear structures can be utilized to obtain a wide bandwidth of the TENG, as well as to boost the output power^[32–35]. For example, Yang et al. reported the use of the multiple-degree and multiple-layer structure based on springs to increase the bandwidth^[36,37]. Besides, to expand the bandwidth, structures based on the nonlinear

spring setup and cantilever beam have also been reported by Guan et al. and Fu et al.^[38,39]. However, in these studies, there are severe friction and collision problems in the proposed TENGs, which lead to a relatively large loss of mechanical energy. At the same time, the systematic studies on the enhancement in the bandwidth brought by the nonlinear structures are still missing.

Here, we propose the addition of a nonlinear restoring force onto an SFT-mode TENG to tune and broaden the frequency bandwidth. The restoring force is applied by permanent magnets at both sides of the slider and two external magnets. A noncontact strategy is adopted between the slider and the grating electrodes to avoid the wearing of the electrodes and energy loss caused by friction. In addition, to make better use of the energy generated by the harvester, we also introduce coils to fabricate electromagnetic generators (EMG) to further enhance the power output. Finally, the harvester can power commercial devices such as a hygrometer by harvesting energy from the environment. This work presents a systematic study to boost the bandwidth and the output power of the TENG enabled by the nonlinear oscillator.

1 Model and principle

The schematic diagram and simulation results of noncontact TENG (NN-TENG) (Figure 1(a)–i) for harvesting vibration energy are illustrated in Figure 1(a). The entire structure is composed of a hollow row frame, which is fabricated by aluminum due to its high rigid, light weight, and non-ferromagnetism. A noncontact SFT mode grating TENG is fixed inside the frame, (Figure 1(a)–ii and Figure 1(a)–iii), and the slider is fabricated by

¹Department of Mechanical and Automation Engineering, The Chinese University of Hong Kong, Shatin, N.T., Hong Kong, China; ²Beijing Institute of Nanoenergy and Nanosystems, Chinese Academy of Sciences, Beijing 100083, China; ³Shenzhen Research Institute, The Chinese University of Hong Kong, Guangdong 518057, China; ⁴HKUST Shenzhen-Hong Kong Collaborative Innovation Research Institute, Guangdong 518048, China; ⁵Thrust of Sustainable Energy and Environment, The Hong Kong University of Science and Technology (Guangzhou), Guangdong 511400, China; ⁶Department of Mechanical and Aerospace Engineering, The Hong Kong University of Science and Technology, Clear Water Bay, Hong Kong, China

Address correspondence to Zhonglin Wang, zhong.wang@mse.gatech.edu; Yunlong Zi, Yunlong Zi, Yunlong Zi, ylzi@ust.hk

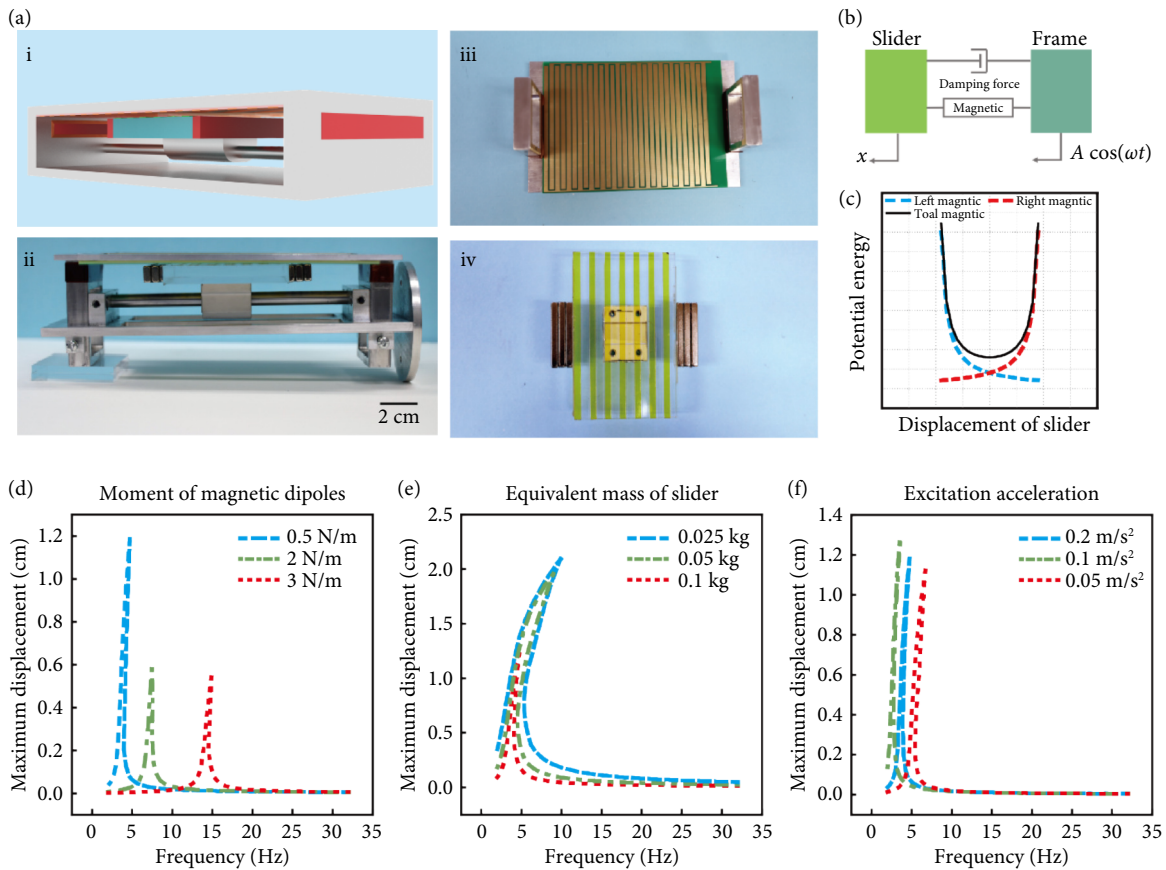


Fig. 1 Schematic illustration and simulation. (a) Schematic and photograph of NN-TENG, (b) potential energy of magnetic dipole, (c) dynamic model of NN-TENG. The amplitude of slider through sweeping mode under different, (d) moment of magnetic dipole, (e) equivalent mass of slider, and (f) excitation acceleration.

an acrylic plate with a Kapton film attached on it as the friction layer (Figure 1(a)–iv). The slider is fixed on a linear bushing and moves on an optical axis rail to minimize the friction as much as possible. In order to decrease wear and friction, a small gap is designed between the slider and the grating electrode to achieve a noncontact SFT mode TENG. Two permanent magnets are attached to the sides of the slider, and these two magnets interact with two fixed magnets located on the frame, resembling the tip magnets. Figure 1(b) shows the schematic of the dynamic model of the whole system, where only inertial, damping, magnetic, and excitation forces are considered. Although electrostatic forces also cause nonlinear behavior, they can be ignored in this work because the magnitude is very small (see Note 1, which is in the Supplementary Information (SI) of the online version of this article). Therefore, the governing equation can be obtained by using Newton's second law:

$$m\ddot{x} + c\dot{x} + F_{\text{mag-T}} = mA\omega^2 \cos(\omega t) \quad (1)$$

where m , c , A , and ω are the equivalent mass, damping, amplitude, and frequency, respectively. Assuming dipole–dipole interactions between the slider and fixed magnets, then the magnetic force between two face-to-face magnets can be written as^[40]

$$F_{\text{mag}} = \frac{3\mu_0 m_1 m_2}{2\pi (x - D_0)^4} \quad (2)$$

where μ_0 is the free space permeability; m_1 and m_2 are the moments of magnetic dipoles of the first and second magnets, respectively; D_0 is the distance between two face-to-face magnets. Note that, for two repulsive magnets, $m_1 \cdot m_2 > 0$, and for two attractive magnets, $m_1 \cdot m_2 < 0$. Considering that the whole structure is symmetrical, the slider at the middle of the frame is set as $x = 0$.

Therefore, the magnitude of the total magnetic force on the slider can be expressed as

$$F_{\text{mag-T}} = \frac{3\mu_0 m_1 m_2}{2\pi (x - D_0)^4} - \frac{3\mu_0 m_1 m_2}{2\pi (x + D_0)^4} \quad (3)$$

Collision problem, as the most energy consuming concern of all vibration energy harvesters, should be avoided as much as possible. This device is designed with no collision because the repulsion force of the magnetic dipole is strong enough at $x = D_0$ or $x = -D_0$, as shown in Figure 1(c).

Moreover, using Taylor series expansion to Eq. (3), the magnitude of the total force can be approximated as

$$F_{\text{mag}} = \mu_0 \frac{m_1 m_2}{\pi D_0^4} \left[12 \frac{x}{D_0} + 60 \left(\frac{x}{D_0} \right)^3 \right] \quad (4)$$

where terms higher than the third order have been neglected. Combining Eq. (1) and Eq. (4), the complete form of the equations describing the dynamics of the NN-TENG can be stated as

$$m\ddot{x} + c\dot{x} + \mu_0 \frac{m_1 m_2}{\pi D_0^4} \left[12 \frac{x}{D_0} + 60 \left(\frac{x}{D_0} \right)^3 \right] = mA\omega^2 \cos(\omega t) \quad (5)$$

Eq. (5) can be used to approximately simulate the vibration modes of the structure under harmonic excitations. In Figures 1(d)–1(e), three different parameters, magnetic force, equivalent mass of slider, and excitation strength, are mainly studied, with all the intermediate parameters given in Table 1, and details of the simulation process are listed in Note 2 and Note 3 in

Table 1 Parameters of the nonlinear TENG

Parameter	Value	Parameter	Value
m	0.1 (kg)	D_0	0.03 (m)
c	0.01 ($\text{N}\cdot\text{s}\cdot\text{m}^{-1}$)	m_1, m_2	0.5 ($\text{A}\cdot\text{m}^2$)
μ_0	$4\pi\times 10^{-7}$ ($\text{N}\cdot\text{A}^{-2}$)	a	0.2 ($\text{m}\cdot\text{s}^{-2}$)

SI. The simulation results show that the strength of the magnetic force can significantly affect the first mode resonance frequency.

2 Results and discussion

2.1 Fabrication

The nonlinear noncontact TENG is fabricated with a printed circuit board (PCB), a mount base, a slider, and two magnetic dipoles. The length and width of the PCB are 165 and 100 mm, respectively, and the thickness is 1.6 mm. For the grating structure, its gap is 2 mm and electrode width is 5 mm. There are a total of 30

electrodes on the PCB, 15 electrodes are positive and others are negative, the width and length of each electrode are 4 and 80 mm, and the gap between electrodes is 2 mm. The thickness of the copper electrode is 50 μm with 5 μm coating to eliminate the oxidation of the copper membrane. The slider is made of an acrylic plate in 10 mm thickness, and a total 7 pieces of 25 μm in thickness. Kapton membrane with the size of 4 mm \times 10 mm is wrapped on the acrylic plate with an interval of 6 mm. Besides, the mount base is fabricated by aluminum, and slider is fixed on the mount base through a linear bushing whose type is SC8UU. Finally, two permanent magnets (50 mm \times 10 mm \times 15 mm) are attached to the sides of the slider, and these two magnets interact with two fixed magnets located on the mount base, resembling the tip magnets, shown in Figure 1(a). As for the linear TENG, the grating electrodes and slider parts are as same as the nonlinear one, while the magnets were removed and two springs were added to the optical axis with a stiffness of about 1000 N/m.

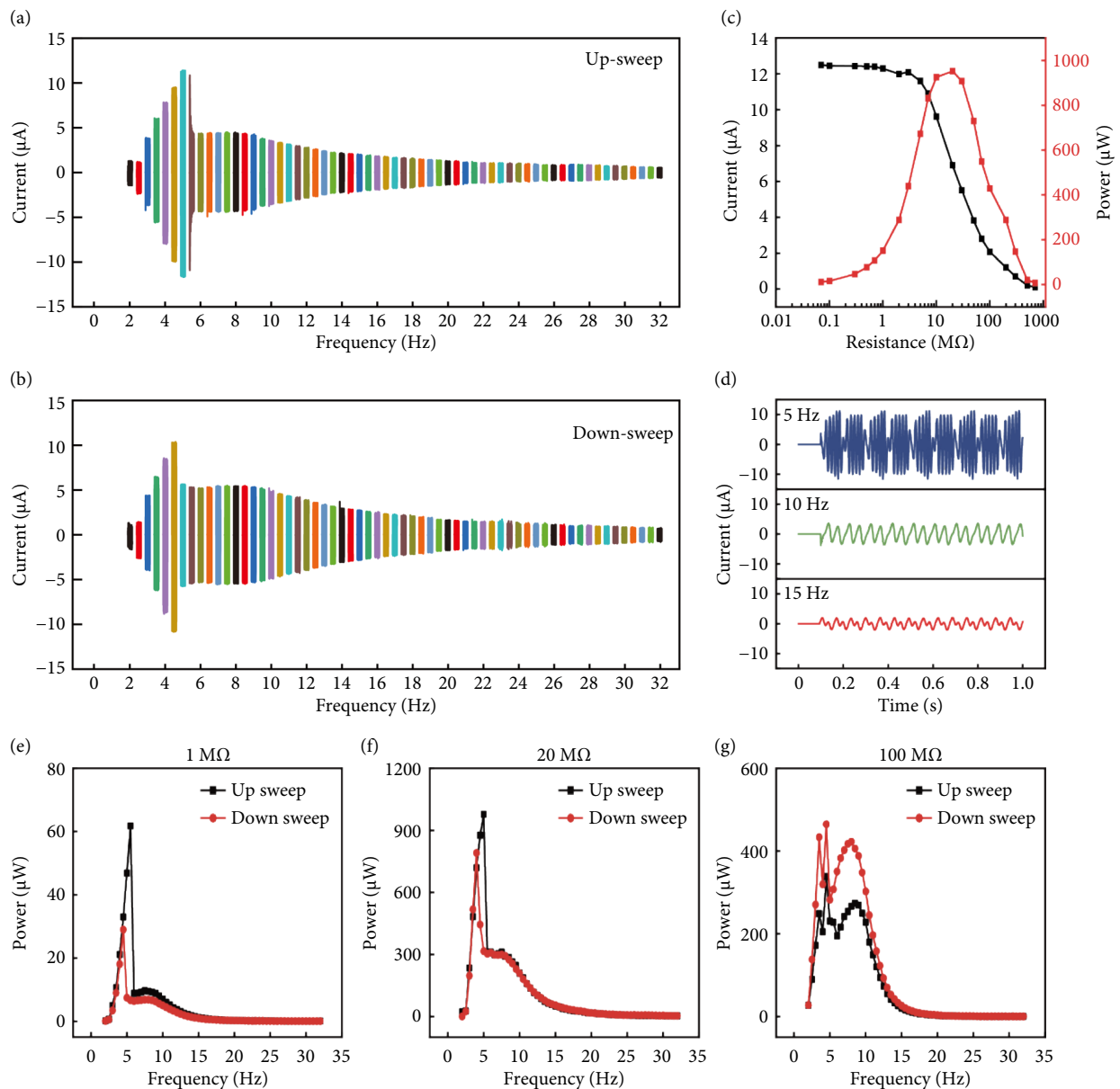


Fig. 2 Electrical output of NN-TENG. (a, b) Current under up-sweep and down-sweep, (c) current and power output under different resistance. (d) Typical current curve under 5 Hz, 10 Hz, and 15 Hz and (e-g) Peak power under 1 $\text{M}\Omega$, 20 $\text{M}\Omega$, and 100 $\text{M}\Omega$.

2.2 Electrical output of NN-TENGs

Based on the simulation results, we fabricate the devices and evaluate the output performance, as shown in Figure 2. Figures 2(a) and 2(b) show the output current from up-sweep with increased frequency and down-sweep with decreased frequency, respectively, where the frequency range is 2–32 Hz, and step size is 0.5 Hz. The results show that there are two common characteristics identified from the current signals. First, the response has a clear and widely broadened response frequency band, which is mostly dominated by the cubic nonlinear term (nonlinear stiffness) of the system, as shown in Eq. (5). Second, there is a distinct jump phenomenon, where the current response abruptly drops or rises as the frequency approaches a specific value (up sweep at 5.5 Hz and down-sweep at 4.5 Hz). It should be noted that the nonlinear system has multiple vibration modes, and the system tends to exhibit different stable states during different scanning processes, resulting in a higher bandwidth.^[12,41,42] Figure 2(c) shows the current and power output under different resistances, where the excitation frequency is 5 Hz. It can be seen that the maximum power output of 1000 μW is reached when external resistance is 20 M Ω . Figure 2(d) shows typical current curves at 5 Hz, 10 Hz, and 15 Hz. The current at 5

Hz has a much higher frequency and amplitude due to the resonance effect. In addition, due to the large amplitude at resonance, the slider can cross multiple grids in one cycle, so that the current frequency is much higher than the resonant frequency. Once the excitation frequency is far away from the resonant frequency, the current output will be correspondingly decreased due to the decreased amplitude of the slider. Besides, external loads also influence the bandwidth. Figures 2(e)–2(g) show the power output performance under 1 M Ω , 20 M Ω , and 100 M Ω by sweeping mode, and the bandwidth gradually increases from 1.5 Hz to 2 Hz and then 7.75 Hz as the external resistance increases. The maximum output power is obtained at the value of the matched impedance of ~ 20 M Ω rather than the maximum resistance, so there are trade-offs to obtain higher power or wider bandwidth.

2.3 Integration and output characteristics of nonlinear electromagnetic generators

Electromagnetic generator (EMG) is a widely used traditional energy harvester. In our system, the role of the magnets is not only to provide a third-order force that generates nonlinearity but also to act as part of EMGs, allowing the entire system to harvest addi-

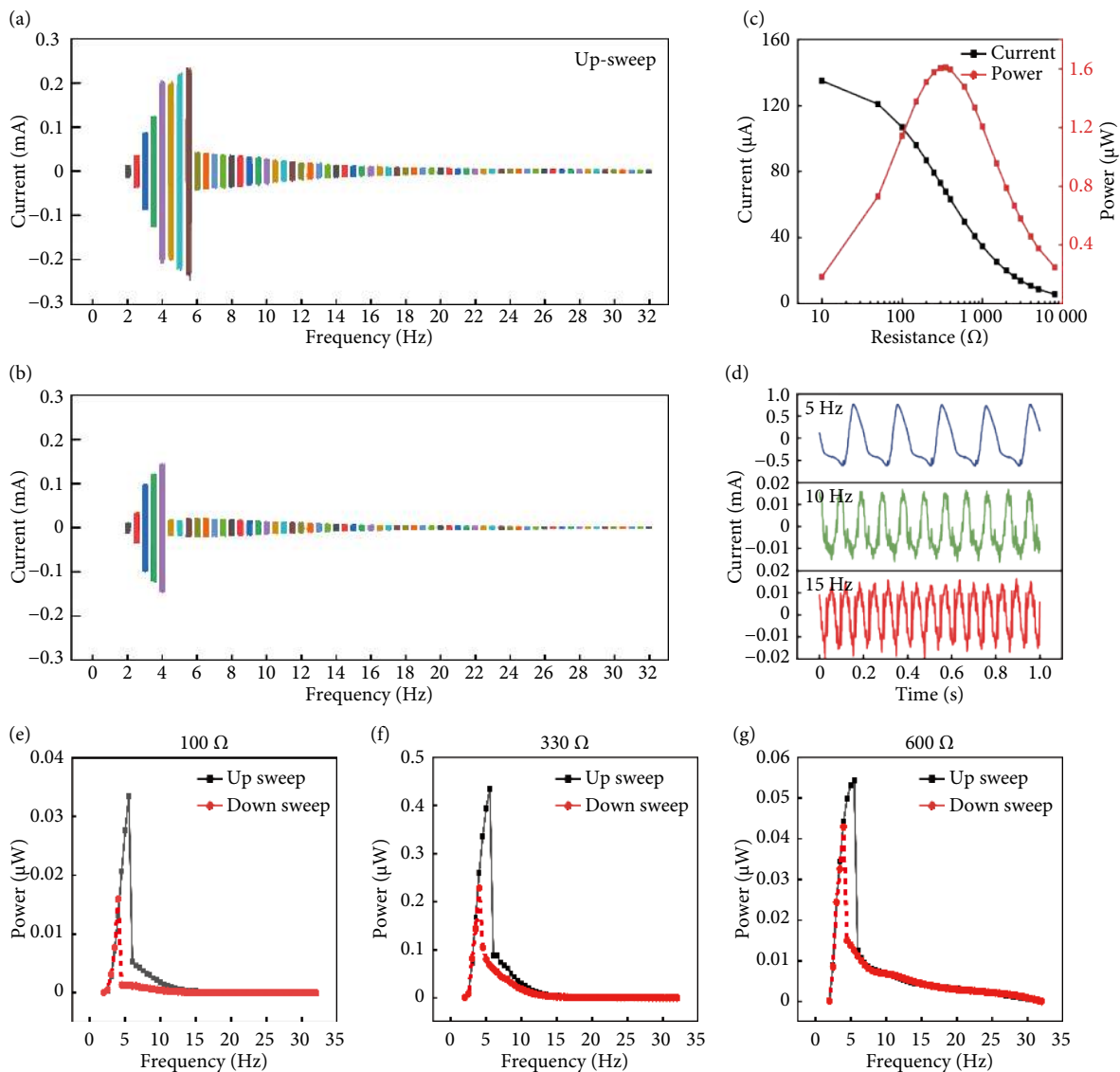


Fig. 3 Electric output of electromagnetic performance. (a, b) Short-circuit current under up-sweep and down-sweep and (c) current and power output under different resistance. (d) Typical current curve under 5 Hz, 10 Hz, and 15 Hz and (e–g) peak power under 100 Ω , 330 Ω , and 600 Ω .

tional energy. As shown in Figure 1(a), the coils are attached to the surface of the magnets by being fixed on the frame, and when the slider vibrates, the magnetic flux through the coils is changing, which results in an AC power output. Figures 3(a) and 3(b) show the short-circuit current under up-sweep and down-sweep, respectively, and it can be clearly seen that the maximum output current generated during the up-sweep is 0.25 mA, which is several times higher than the maximum short-circuit current of TENG. However, the matching impedance of the EMG is low, causing its current to be heavily influenced by external loads, as shown in Figure 3(c). As the external resistance increases from 10 Ω to 10 k Ω , the current decays from the initial 135 μ A to 3 μ A, and the maximum output reaches 1.6 μ W when the external resistance is equal to 330 Ω . Figure 3(c) shows the power output of EMG under up-sweep and down-sweep, where external resistance is 330 Ω . Figure 3(d) shows the typical current outputs under 5 Hz, 10 Hz, and 15 Hz, while the maximum output is obtained around 5 Hz as the resonant frequency. Figures 3(e)–3(g) show the power output performance under 100 Ω , 330 Ω , and 600 Ω by sweeping

mode, and the bandwidth gradually increases from 1.5 Hz to 2 Hz and then 4 Hz as the external resistance increases. The maximum output power is obtained at the value of the matched impedance of around 330 Ω rather than the maximum resistance, so there are some trade-offs to obtaining higher power or wider bandwidth. Such low-impedance output from the integrated EMGs may serve as a supplement to the output performance of the NN-TENG.

2.4 Comparison between the linear and nonlinear TENGs

Finally, we compare the output performances of linear systems (see Supporting Information Note 4) and nonlinear systems, as given in Table 2, where power density is defined as power divided by energy conversion part volume. We define half of the peak power of each system as the reference power to identify the bandwidth, which is defined as the frequency range when the output power of the collector is greater than or equal to the reference power. The results show that compared with the linear system, the nonlinear noncontact TENG (NN-TENG) can increase the peak current from 6.3 μ A to 7.89 μ A, with an increment of about 25 %;

Table 2 Comparisons of peak current, peak power density, and bandwidth

	Linear-TENG		Nonlinear-TENG		Nonlinear-EMG		
	20 M Ω	1 M Ω	20 M Ω	100 M Ω	100 Ω	330 Ω	600 Ω
Resistance	20 M Ω	1 M Ω	20 M Ω	100 M Ω	100 Ω	330 Ω	600 Ω
Peak current (μ A)	6.3	7.86	6.99	2.16	18.57	36.31	9.75
Peak power density (W/m ³)	25.4	2.42	38.2	18.2	1.3	17.0	2.2
Bandwidth (Hz)	0.5	1.5	2	7.75	1.5	2	4

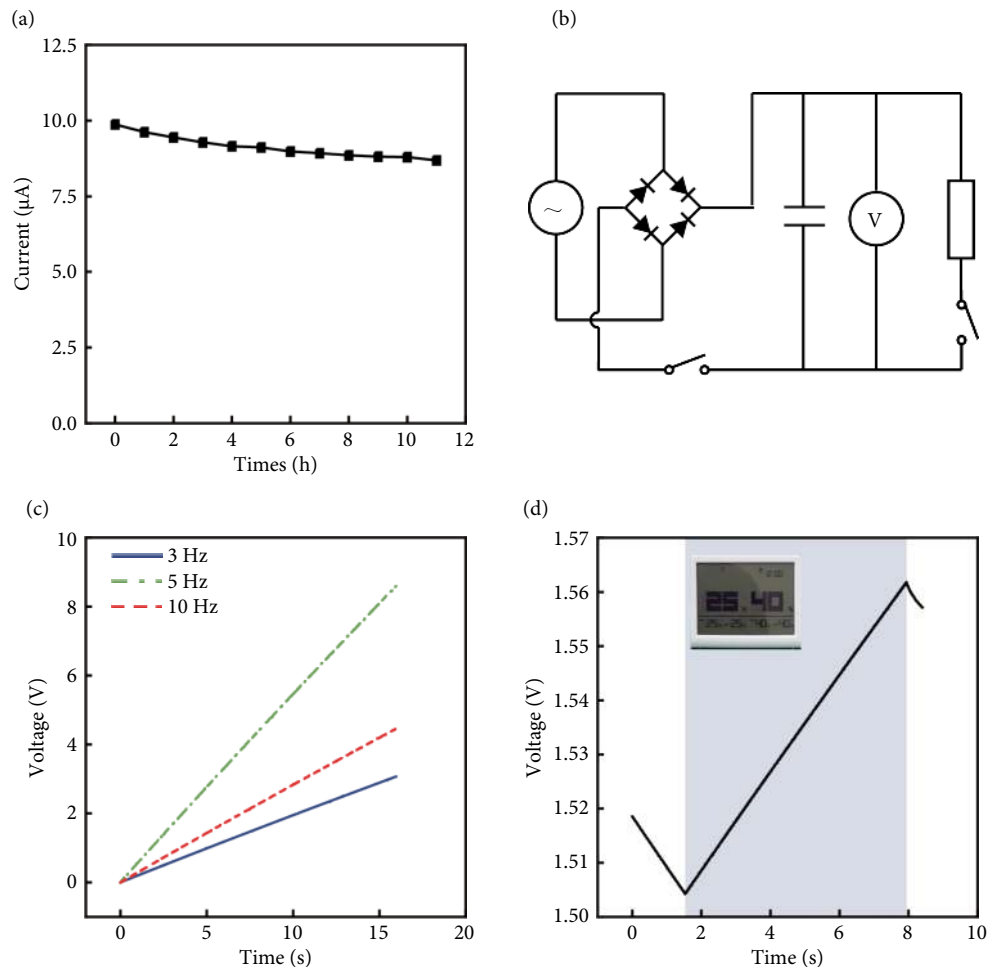


Fig. 4 Application of NN-TENG. (a) Current decay with time, (b) the equivalent circuit diagram of the self-powered system for powering various electronic devices, (c) charging curves of the capacitor by the TENG, and (d) the hygrometer powered by the TENG.

it can increase the peak power from 650 μW to 977 μW , increasing by about 50%; and the bandwidth is increased from 0.5 Hz to 7.75 Hz, increasing by about 1400%.

2.5 Demonstration of applications

The high-performance output delivered by the NN-TENG is demonstrated for different applications. Figure 4(a) shows the current change of the NN-TENG working continuously for over ten hours. Although it is a noncontact form, the charge on the Kapton surface can exist for a long time, which makes this design meet the needs without the severe charge decay issue. Figure 4(b) is the circuit diagram of the self-powered system integrating a TENG and a capacitor by a full wave rectifier. Operating by the shaker at a frequency of 3 Hz, 5 Hz, and 10 Hz, the 10 μF capacitor can reach 3 V, 9 V, and 5 V after 15 s, as shown in Figure 4(c). Furthermore, Figure 4(d) presents an electronic hygrometer powered by manually pressing the NN-TENG (Supplementary Video 1). When the NN-TENG is triggered by a shaker, an electronic hygrometer can be sustainably lit up by walking (Supplementary Video 1). Moreover, the TENG with high output performance may have great potential for application in air purification, electrostatic adsorption, etc.

3 Conclusions

In summary, a nonlinear noncontact oscillator-based grating TENG is proposed to boost its output performance, which is achieved by the nonlinear restoring magnetic force. The theoretical model to capture the dynamic responses is established. Through this model, we predict that the power output can be enhanced by the nonlinear property of the magnetic force. In addition, the integrated EMG enabled by the magnetic force and coils demonstrates low-impedance output characteristics, which can serve as a supplement to the high-impedance TENG output to enable wider applications. Compared with the traditional linear vibration system, the nonlinear oscillator-based TENG has the advantages of high-power output, wide bandwidth, and compact structure. This work may open a new method to harvest broadband vibrational energy with high output performance to power multiple devices for the Internet of Things and other applications.

Acknowledgements

This work was supported by HKSAR the Research Grants Council Early Career Scheme (Grant No. 24206919), and Guangdong Basic and Applied Basic Research Foundation (Project No. 2020A1515111161). This work was supported in part by the Project of Hetao Shenzhen-Hong Kong Science and Technology Innovation Cooperation Zone (HZQB-KCZYB-2020083).

Article history

Received: 29 June 2022; Revised: 27 July 2022; Accepted: 29 July 2022

Additional information

Supplementary information The online version contains supplementary material available at <https://doi.org/10.23919/IEN.2022.0028>.

© 2022 The Author(s). This is an open access article under the CC BY license (<http://creativecommons.org/licenses/by/4.0/>).

Declaration of competing interest

The authors have no competing interests to declare that are relevant to the content of this article.

References

- [1] Wang, Z. L. (2019). Entropy theory of distributed energy for internet of things. *Nano Energy*, 58: 669–672.
- [2] Luo, J. J., Gao, W. C., Wang, Z. L. (2021). The triboelectric nanogenerator as an innovative technology toward intelligent sports. *Advanced Materials*, 33: 2004178.
- [3] Wu, C. S., Wang, A. C., Ding, W. B., Guo, H. Y., Wang, Z. L. (2019). Triboelectric nanogenerator: A foundation of the energy for the new era. *Advanced Energy Materials*, 9: 1802906.
- [4] Chu, S., Majumdar, A. (2012). Opportunities and challenges for a sustainable energy future. *Nature*, 488: 294–303.
- [5] Luo, J. J., Wang, Z. L. (2020). Recent progress of triboelectric nanogenerators: From fundamental theory to practical applications. *Eco-Mat*, 2: e12059.
- [6] Ahmed, A., Hassan, I., Ibn-Mohammed, T., Mostafa, H., Reaney, I. M., Koh, L. S. C., Zu, J., Wang, Z. L. (2017). Environmental life cycle assessment and techno-economic analysis of triboelectric nanogenerators. *Energy & Environmental Science*, 10: 653–671.
- [7] Wang, Z. L. (2017). Catch wave power in floating nets. *Nature*, 542: 159–160.
- [8] Wang, H. M., Xu, L., Wang, Z. L. (2021). Advances of high-performance triboelectric nanogenerators for blue energy harvesting. *Nanoenergy Advances*, 1: 32–57.
- [9] Wang, Z. L., Jiang, T., Xu, L. (2017). Toward the blue energy dream by triboelectric nanogenerator networks. *Nano Energy*, 39: 9–23.
- [10] Wei, C. F., Jing, X. J. (2017). A comprehensive review on vibration energy harvesting: Modelling and realization. *Renewable and Sustainable Energy Reviews*, 74: 1–18.
- [11] Yang, Z. B., Erturk, A., Zu, J. (2017). On the efficiency of piezoelectric energy harvesters. *Extreme Mechanics Letters*, 15: 26–37.
- [12] Wang, Y. L., Yang, Z. B., Li, P. Y., Cao, D. Q., Huang, W. H., Inman, D. J. (2020). Energy harvesting for jet engine monitoring. *Nano Energy*, 75: 104853.
- [13] Ye, C. Y., Dong, K., An, J., Yi, J., Peng, X., Ning, C., Wang, Z. L. (2021). A triboelectric–electromagnetic hybrid nanogenerator with broadband working range for wind energy harvesting and a self-powered wind speed sensor. *ACS Energy Letters*, 6: 1443–1452.
- [14] Zhang, C., Tang, W., Han, C. B., Fan, F. R., Wang, Z. L. (2014). Theoretical comparison, equivalent transformation, and conjunction operations of electromagnetic induction generator and triboelectric nanogenerator for harvesting mechanical energy. *Advanced Materials*, 26: 3580–3591.
- [15] Williams, C. B., Shearwood, C., Harradine, M. A., Mellor, P. H., Birch, T. S., Yates, R. B. (2001). Development of an electromagnetic micro-generator. *IEE Proceedings – Circuits, Devices and Systems*, 148: 337–342.
- [16] Zhang, K. W., Wang, X., Yang, Y., Wang, Z. L. (2015). Hybridized electromagnetic–triboelectric nanogenerator for scavenging biomechanical energy for sustainably powering wearable electronics. *ACS Nano*, 9: 3521–3529.
- [17] Fu, J. J., Xu, G. Q., Li, C. H., Xia, X., Guan, D., Li, J., Huang, Z. Y., Zi, Y. L. (2020). Achieving ultrahigh output energy density of triboelectric nanogenerators in high-pressure gas environment. *Advanced Science*, 7: 2001757.
- [18] Li, X. Y., Zhang, C. G., Gao, Y. K., Zhao, Z. H., Hu, Y. X., Yang, O., Liu, L., Zhou, L. L., Wang, J., Wang, Z. L. (2022). A highly efficient constant-voltage triboelectric nanogenerator. *Energy & Environmental Science*, 15: 1334–1345.
- [19] Wu, H., Wang, S., Wang, Z. K., Zi, Y. L. (2021). Achieving ultrahigh instantaneous power density of 10 MW/m² by leveraging the opposite-charge-enhanced transistor-like triboelectric nanogenerator (OCT-TENG). *Nature Communications*, 12: 5470.

- [20] Wang, Z. L. (2020). On the first principle theory of nanogenerators from Maxwell's equations. *Nano Energy*, 68: 104272.
- [21] Wang, Z. L. (2017). On Maxwell's displacement current for energy and sensors: The origin of nanogenerators. *Materials Today*, 20: 74–82.
- [22] Wang, Z. L. (2022). On the expanded Maxwell's equations for moving charged media system—General theory, mathematical solutions and applications in TENG. *Materials Today*, 52: 348–363.
- [23] Zou, Y. J., Raveendran, V., Chen, J. (2020). Wearable triboelectric nanogenerators for biomechanical energy harvesting. *Nano Energy*, 77: 105303.
- [24] Chen, B., Yang, Y., Wang, Z. L. (2018). Scavenging wind energy by triboelectric nanogenerators. *Advanced Energy Materials*, 8: 1702649.
- [25] Wu, H., Wang, Z. K., Zi, Y. L. (2021). Multi-mode water-tube-based triboelectric nanogenerator designed for low-frequency energy harvesting with ultrahigh volumetric charge density. *Advanced Energy Materials*, 11: 2100038.
- [26] Zi, Y. L., Guo, H. Y., Wen, Z., Yeh, M. H., Hu, C. G., Wang, Z. L. (2016). Harvesting low-frequency (< 5 Hz) irregular mechanical energy: a possible killer application of triboelectric nanogenerator. *ACS Nano*, 10: 4797–4805.
- [27] Dong, K., Wang, Z. L. (2021). Self-charging power textiles integrating energy harvesting triboelectric nanogenerators with energy storage batteries/supercapacitors. *Journal of Semiconductors*, 42: 101601.
- [28] Niu, S. M., Wang, Z. L. (2015). Theoretical systems of triboelectric nanogenerators. *Nano Energy*, 14: 161–192.
- [29] Wang, Z. L., Wang, A. C. (2019). On the origin of contact-electrification. *Materials Today*, 30: 34–51.
- [30] Fu, J. J., Xia, X., Xu, G. Q., Li, X. Y., Zi, Y. L. (2019). On the maximal output energy density of nanogenerators. *ACS Nano*, 13: 13257–13263.
- [31] Yu, H., He, X., Ding, W. B., Hu, Y. S., Yang, D. C., Lu, S., Wu, C. S., Zou, H. Y., Liu, R. Y., Lu, C. H., et al. (2017). A self-powered dynamic displacement monitoring system based on triboelectric accelerometer. *Advanced Energy Materials*, 7: 1700565.
- [32] Tadesse, Y., Zhang, S. J., Priya, S. (2009). Multimodal energy harvesting system: Piezoelectric and electromagnetic. *Journal of Intelligent Material Systems and Structures*, 20: 625–632.
- [33] Zhu, J. X., Wang, A. C., Hu, H. B., Zhu, H. (2017). Hybrid electro-magnetic and triboelectric nanogenerators with multi-impact for wideband frequency energy harvesting. *Energies*, 10: 2024.
- [34] Li, Z. J., Saadatnia, Z., Yang, Z. B., Naguib, H. (2018). A hybrid piezoelectric-triboelectric generator for low-frequency and broadband energy harvesting. *Energy Conversion and Management*, 174: 188–197.
- [35] Tang, G., Cheng, F., Hu, X., Huang, B., Xu, B., Li, Z. B., Yan, X. X., Yuan, D. D., Wu, W. J., Shi, Q. F. (2019). A two-degree-of-freedom cantilever-based vibration triboelectric nanogenerator for low-frequency and broadband operation. *Electronics*, 8: 1526.
- [36] Yang, W. Q., Chen, J., Jing, Q. S., Yang, J., Wen, X. N., Su, Y. J., Zhu, G., Bai, P., Wang, Z. L. (2014). 3D stack integrated triboelectric nanogenerator for harvesting vibration energy. *Advanced Functional Materials*, 24: 4090–4096.
- [37] Yang, J., Chen, J., Yang, Y., Zhang, H. L., Yang, W. Q., Bai, P., Su, Y. J., Wang, Z. L. (2014). Broadband vibrational energy harvesting based on a triboelectric nanogenerator. *Advanced Energy Materials*, 4: 1301322.
- [38] Guan, D., Xu, G. Q., Xia, X., Wang, J. Q., Zi, Y. L. (2021). Boosting the output performance of the triboelectric nanogenerator through the nonlinear oscillator. *ACS Applied Materials & Interfaces*, 13: 6331–6338.
- [39] Fu, Y. Q., Ouyang, H. J., Davis, R. B. (2018). Nonlinear dynamics and triboelectric energy harvesting from a three-degree-of-freedom vibro-impact oscillator. *Nonlinear Dynamics*, 92: 1985–2004.
- [40] Rezaei, M., Talebitooti, R., Friswell, M. I. (2019). Efficient acoustic energy harvesting by deploying magnetic restoring force. *Smart Materials and Structures*, 28: 105037.
- [41] Zou, D. L., Liu, G. Y., Rao, Z. S., Zi, Y. L., Liao, W. H. (2021). Design of a broadband piezoelectric energy harvester with piecewise nonlinearity. *Smart Materials and Structures*, 30: 085040.
- [42] Sebald, G., Kuwano, H., Guyomar, D., Ducharme, B. (2011). Experimental duffing oscillator for broadband piezoelectric energy harvesting. *Smart Materials and Structures*, 20: 102001.